



Natural convective flow between isothermal concentric spheres  
by Shiu-hau Yin

A dissertation submitted to the Graduate Faculty in partial fulfillment of the requirements for the degree of DOCTOR OF PHILOSOPHY in Aerospace and Mechanical Engineering  
Montana State University  
© Copyright by Shiu-hau Yin (1972)

**Abstract:**

Natural convective flow of air and water between isothermal concentric spheres was experimentally investigated. Different visualization techniques were utilized for each specified fluid. A special visualization technique was developed for water as the working medium in this study. The visualization of the flow pattern was accomplished by introducing a well mixed and prepared solution of distilled water containing a very minute amount of liquid "Ajax" detergent into the annulus and transversely illuminating vertical diameter.

For air in the gap, smoke was introduced. A qualitative description of the flow patterns obtained for each spherical combination studied is presented, and these descriptions are supplemented by photographs of the flow. Motion pictures of each distinctive type of flow pattern found to occur in this investigation were also obtained.

For air as the working fluid, distinct steady and unsteady patterns were obtained for various diameter ratios ranging from 1.40 to 2.17 and for Grashof numbers (based on gap thickness) ranging from  $7.0 \times 10^3$  to  $1.2 \times 10^6$ . The flow patterns at the lower Grashof numbers qualitatively agree with those obtained in previous studies. The inception of instabilities characterized by periodic interior contractions or three-dimensional spiral flow in the spherical annuli was compared to the case of horizontal cylindrical annuli.

For water as working fluid, the most common basic flow pattern, the steady dog-face type, occurred in the three largest diameter ratios investigated. This kind of flow pattern has never been observed before, but it does correlate quite well with the temperature profiles obtained in the heat transfer study. A formation of tertiary flow in the weak shear layer between two secondary cells occurred for the diameter ratio of 1.78 ( $L/D_i=0.39$ ) at high Grashof numbers. As the Grashof number was increased above certain transition points, an unsteady dog—face type flow, or a three-dimensional spiral flow, was observed. In this study, the diameter ratio ranged from 1.09 to 2.17 and the Grashof number based on gap thickness ranged from  $1.7 \times 10^3$  to  $1.4 \times 10^7$ .

A tabular form of the experimental results for each test fluid is presented to provide categorization of the fluid-flow behavior within the available ranges of independent variables.

NATURAL CONVECTIVE FLOW BETWEEN  
ISOTHERMAL CONCENTRIC SPHERES

by

SHIU-HAU YIN  
✓

A dissertation submitted to the Graduate Faculty  
in partial fulfillment of the requirements for the degree

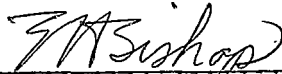
of

DOCTOR OF PHILOSOPHY

in

Aerospace and Mechanical Engineering

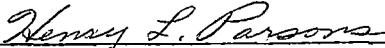
Approved:



Head, Major Department



Chairman, Examining Committee



Graduate Dean

MONTANA STATE UNIVERSITY  
Bozeman, Montana

March, 1972

## ACKNOWLEDGEMENT

The author wishes to express his sincere thanks and appreciation to all those who have aided in this work. Special thanks are due to Dr. J. A. Scanlan, Dr. E. H. Bishop, and Dr. R. E. Powe for their advice, guidance, and encouragement. Thanks also go to Mr. Gordon Williamson for his assistance in constructing the entire apparatus. The writer is especially appreciative of the patience and understanding of his wife, Sandra.

The work reported in this thesis was supported by the Atomic Energy Commission under Contract Number AT(45-1)-2214.

## TABLE OF CONTENTS

Chapter	Page
VITA . . . . .	ii
ACKNOWLEDGEMENT . . . . .	iii
LIST OF TABLES . . . . .	v
LIST OF FIGURES . . . . .	vi
ABSTRACT . . . . .	x
NOMENCLATURE . . . . .	xi
I. INTRODUCTION . . . . .	1
II. LITERATURE REVIEW . . . . .	4
III. EXPERIMENTAL SYSTEM . . . . .	17
APPARATUS . . . . .	17
PROCEDURE . . . . .	34
IV. EXPERIMENTAL RESULTS AND DISCUSSION . . . . .	39
FLOW PATTERN DESCRIPTIONS . . . . .	41
SUMMARY OF EXPERIMENTAL RESULTS . . . . .	86
DISCUSSION OF RESULTS . . . . .	94
V. CONCLUSIONS AND RECOMMENDATIONS . . . . .	103
APPENDIX I. GOVERNING DIFFERENTIAL EQUATIONS . . . . .	107
APPENDIX II. EQUIPMENT LIST . . . . .	112
APPENDIX III. COMPUTER PROGRAMS . . . . .	115
BIBLIOGRAPHY . . . . .	126

## LIST OF TABLES

Table	Page
1. Gap Working Fluid and Associated Geometric Combinations . . . . .	38
2. Summary of Results for Air as the Gap Working Fluid . . . .	89
3. Summary of Results for Water as the Gap Working Fluid . .	92

## LIST OF FIGURES

Figure	Page
1. Assembled Apparatus with Water Cooling System . . . . .	18
2. Schematic Diagram of Experimental System (Water as Gap Fluid) . . . . .	19
3. Schematic Diagram of Experimental System (Air as Gap Fluid) . . . . .	20
4. Interior of Inner Sphere . . . . .	22
5. Glass Hemispheres . . . . .	24
6. Installation of Inner Sphere Inside the Glass Sphere . . .	25
7. Particles in Water within the Spherical Annulus before Heating . . . . .	31
8. Steady Crescent Eddy Pattern for $D_o/D_i = 2.17$ , $L/D_i =$ $0.59$ , $N_{GR_L} = 72,000$ , $N_{RA_L} = 51,000$ . . . . .	42
9. Photograph Showing Onset of Steady Kidney-Shaped Eddy Pattern for $D_o/D_i = 2.17$ , $L/D_i = 0.59$ , $N_{GR_L} =$ $166,500$ , $N_{RA_L} = 118,000$ . . . . .	44
10. Steady Kidney-Shaped Eddy Pattern for $D_o/D_i = 2.17$ $L/D_i = 0.59$ , $N_{GR_L} = 295,800$ , $N_{RA_L} = 209,600$ . . . . .	45
11. Steady Kidney-Shaped Eddy Pattern for $D_o/D_i = 2.17$ , $L/D_i =$ $0.59$ , $N_{GR_L} = 555,000$ , $N_{RA_L} = 393,000$ . . . . .	47
12. Steady Modified Kidney-Shaped Eddy Pattern for $D_o/D_i = 2.17$ , $L/D_i = 0.59$ , $N_{GR_L} = 1,056,000$ , $N_{RA_L} = 746,000$ . . . . .	48
13. Steady Crescent Eddy Pattern for $D_o/D_i = 1.78$ , $L/D_i =$ $0.39$ , $N_{GR_L} = 93,100$ , $N_{RA_L} = 66,000$ . . . . .	50

Figure	Page
14. Steady Kidney-Shaped Eddy Pattern for $D_o/D_i = 1.78$ , $L/D_i = 0.39$ , $N_{GR_L} = 194,000$ , $N_{RA_L} = 137,400$ . . . . .	51
15. Photograph of Flow Pattern for $D_o/D_i = 1.78$ , $L/D_i = 0.39$ , $N_{GR_L} = 246,700$ , $N_{RA_L} = 174,600$ . . . . .	53
16. Photograph of Flow Pattern for $D_o/D_i = 1.78$ , $L/D_i = 0.39$ , $N_{GR_L} = 275,000$ , $N_{RA_L} = 194,600$ . . . . .	54
17. Periodic Interior Contraction Flow for $D_o/D_i = 1.78$ , $L/D_i = 0.39$ , $N_{GR_L} = 323,000$ , $N_{RA_L} = 228,400$ . . . . .	55
18. Sketch of Flow Pattern for $D_o/D_i = 1.40$ , $L/D_i = 0.20$ , $N_{GR_L} = 8,400$ , $N_{RA_L} = 5,950$ . . . . .	57
19. Photograph of Flow Pattern for $D_o/D_i = 1.40$ , $L/D_i = 0.20$ , $N_{GR_L} = 8,400$ , $N_{RA_L} = 5,950$ . . . . .	58
20. Steady Crescent Eddy Pattern for $D_o/D_i = 1.40$ , $L/D_i = 0.20$ $N_{GR_L} = 25,000$ , $N_{RA_L} = 17,700$ . . . . .	59
21. Photograph of Flow Pattern for $D_o/D_i = 1.40$ , $L/D_i = 0.20$ , $N_{GR_L} = 99,300$ , $N_{RA_L} = 70,000$ . . . . .	61
22. Photograph Showing Counter Rotating Cells in Upper Region of Annulus for $D_o/D_i = 1.40$ , $L/D_i = 0.20$ , $N_{GR_L} = 103,800$ , $N_{RA_L} = 73,200$ . . . . .	63
23. Photograph Showing Counter Rotating Cells in Upper Region of Annulus for $D_o/D_i = 1.40$ , $L/D_i = 0.20$ , $N_{GR_L} = 103,800$ , $N_{RA_L} = 73,200$ . . . . .	64
24. Three-Dimensional Spiral Motion in Upper Gap Region for $D_o/D_i = 1.40$ , $L/D_i = 0.20$ , $N_{GR_L} = 103,800$ , $N_{RA_L} = 73,200$ . . . . .	65

Figure	Page
25. Sketch of Steady Dog-Face Pattern for $D_o/D_i = 2.17$ , $L/D_i = 0.59$ , $N_{GR_L} = 248,800$ , $N_{RA_L} = 2,812,000$ . . . . .	67
26. Steady Dog-Face Pattern for $D_o/D_i = 2.17$ , $L/D_i = 0.59$ , $N_{GR_L} = 248,800$ , $N_{RA_L} = 2,812,000$ . . . . .	68
27. Steady Dog-Face Pattern (Upper Portion) for $D_o/D_i = 2.17$ , $L/D_i = 0.59$ , $N_{GR_L} = 248,800$ , $N_{RA_L} = 2,812,000$ . . . . .	69
28. Photograph of Flow Pattern for $D_o/D_i = 2.17$ , $L/D_i = 0.59$ , $N_{GR_L} = 1,345,000$ , $N_{RA_L} = 12,554,000$ . . . . .	71
29. Steady Dog-Face Pattern for $D_o/D_i = 1.78$ , $L/D_i = 0.39$ , $N_{GR_L} = 404,000$ , $N_{RA_L} = 3,992,000$ . . . . .	73
30. Sketch of Tertiary Flow Pattern for $D_o/D_i = 1.78$ , $L/D_i = 0.39$ , $N_{GR_L} = 1,688,000$ , $N_{RA_L} = 14,170,000$ . . . . .	75
31. Tertiary Flow Pattern (Upper Portion) for $D_o/D_i = 1.78$ , $L/D_i = 0.39$ , $N_{GR_L} = 1,688,000$ , $N_{RA_L} = 14,170,000$ . . . . .	76
32. Tertiary Flow Pattern (Upper Portion) for $D_o/D_i = 1.78$ , $L/D_i = 0.39$ , $N_{GR_L} = 1,688,000$ , $N_{RA_L} = 14,170,000$ . . . . .	77
33. Steady Dog-Face Pattern (Upper Portion) for $D_o/D_i = 1.40$ , $L/D_i = 0.20$ , $N_{GR_L} = 117,000$ , $N_{RA_L} = 1,115,000$ . . . . .	78
34. Photograph of Flow Pattern (Upper Portion) for $D_o/D_i = 1.40$ , $L/D_i = 0.20$ , $N_{GR_L} = 1,224,000$ , $N_{RA_L} = 8,322,000$ . . . . .	80
35. Three-Dimensional Spiral Motion in Upper Gap Region for $D_o/D_i = 1.40$ , $L/D_i = 0.20$ , $N_{GR_L} = 2,497,000$ , $N_{RA_L} = 14,946,000$ . . . . .	82

Figure	Page
36. Photograph of Flow Pattern (Upper Portion) for $D_o/D_i$ = 1.09, $L/D_i = 0.04$ , $N_{GR_L} = 1,840$ , $N_{RA_L} = 18,300$ . . .	84
37. Photograph of Flow Pattern (Lower Portion) for $D_o/D_i$ = 1.09, $L/D_i = 0.04$ , $N_{GR_L} = 1,840$ , $N_{RA_L} = 18,300$ . . .	85
38. Temperature Profiles for Water, $D_o/D_i = 1.40$ , $L/D_i =$ 0.20, $N_{GR_L} = 1,217,000$ , $N_{RA_L} = 7,923,000$ . . . . .	99
39. Sketch of Steady Dog-Face Pattern for $D_o/D_i = 1.40$ , $L/D_i = 0.20$ , $N_{GR_L} = 1,217,000$ , $N_{RA_L} = 7,923,000$ . . .	100

## ABSTRACT

Natural convective flow of air and water between isothermal concentric spheres was experimentally investigated. Different visualization techniques were utilized for each specified fluid. A special visualization technique was developed for water as the working medium in this study. The visualization of the flow pattern was accomplished by introducing a well mixed and prepared solution of distilled water containing a very minute amount of liquid "Ajax" detergent into the annulus and transversely illuminating vertical diameter. For air in the gap, smoke was introduced. A qualitative description of the flow patterns obtained for each spherical combination studied is presented, and these descriptions are supplemented by photographs of the flow. Motion pictures of each distinctive type of flow pattern found to occur in this investigation were also obtained.

For air as the working fluid, distinct steady and unsteady patterns were obtained for various diameter ratios ranging from 1.40 to 2.17 and for Grashof numbers (based on gap thickness) ranging from  $7.0 \times 10^3$  to  $1.2 \times 10^6$ . The flow patterns at the lower Grashof numbers qualitatively agree with those obtained in previous studies. The inception of instabilities characterized by periodic interior contractions or three-dimensional spiral flow in the spherical annuli was compared to the case of horizontal cylindrical annuli.

For water as working fluid, the most common basic flow pattern, the steady dog-face type, occurred in the three largest diameter ratios investigated. This kind of flow pattern has never been observed before, but it does correlate quite well with the temperature profiles obtained in the heat transfer study. A formation of tertiary flow in the weak shear layer between two secondary cells occurred for the diameter ratio of 1.78 ( $L/D_i=0.39$ ) at high Grashof numbers. As the Grashof number was increased above certain transition points, an unsteady dog-face type flow, or a three-dimensional spiral flow, was observed. In this study, the diameter ratio ranged from 1.09 to 2.17 and the Grashof number based on gap thickness ranged from  $1.7 \times 10^3$  to  $1.4 \times 10^7$ .

A tabular form of the experimental results for each test fluid is presented to provide categorization of the fluid-flow behavior within the available ranges of independent variables.

## NOMENCLATURE

Symbol	Description
a, b	Characteristic physical dimensions
$C_p$	Fluid specific heat at constant pressure
D	Diameter
g	Acceleration of gravity, 32.174 ft/sec <sup>2</sup>
H	Height of vertical plate
k	Fluid thermal conductivity
L	Distance between plates; gap thickness (difference between outer and inner spherical radii)
$N_D$	Characteristic physical dimension ratio
$N_{GR_a}$	Grashof number, $\rho^2 g \beta (T_i - T_o) a^3 / \mu^2$ , a is replaced by any desired characteristic dimension
$N_{PR}$	Prandtl number, $C_p \mu / k$
$N_{RA_a}$	Rayleigh number, $\rho^2 g \beta (T_i - T_o) a^3 C_p / \mu k$
r	Radial coordinate
$r_{avg}$	Average radius, $r_{avg} = (r_i + r_o) / 2$
T	Temperature
$\Delta T$	Temperature difference between inner and outer spheres, $T_i - T_o$
$\alpha$	Thermal Diffusivity, $k / \rho C_p$
$\beta$	Thermal expansion coefficient
$\phi$	Angular coordinate measured from upward vertical axis

Symbol	Description
$\mu$	Dynamic viscosity of the fluid
$\rho$	Fluid density

Subscripts

am	Arithmetic mean
i	Refers to inner sphere
L	Based on distance between plates or gap thickness
o	Refers to outer sphere
vm	Volume weighted mean

## CHAPTER I

### INTRODUCTION

In recent years, a considerable amount of interest has developed in the subject of natural convection from a body to its finite enclosure. This particular heat transfer and fluid mechanics problem is becoming increasingly important in certain areas such as nuclear design, aircraft cabin design, and electronic instrumentation packaging. However, only relatively little information has been reported in this area.

Since 1964, an important beginning in this broad area has been made in the study of natural convection between concentric isothermal spheres. The first investigation, using air as the gap fluid, was carried out by Bishop, Kolflat, Mack, and Scanlan [1]. Utilizing the techniques reported in [2], they described the flow patterns observed visually and photographically. Heat transfer data, temperature distributions, and additional comments on the flow patterns were presented by Bishop et al [3]. An analytical prediction of both thermal and flow fields by Mack and Hardee [4] is valid only for low Rayleigh numbers. The most recent studies are those of Scanlan, Bishop, and Powe [5], and Weber, Powe, Bishop, and Scanlan [6]. They extended the existing heat transfer data and temperature distributions of Bishop et al [3] ( $N_{PR} \sim 0.7$ ) to include Prandtl numbers up to 4184 by using water and two silicone fluids as

working media for both concentric and vertically eccentric cases.

Unfortunately, most of these previous studies are restricted to the heat transfer rates and temperature fields; there is little information available concerning the flow field of this specific geometrical configuration. In order to fully understand the convection process, both thermal and flow phenomena must be known. Therefore, the purpose of the current investigation is to attempt to alleviate the problem of the serious lack of knowledge of the flow behavior in this particular geometry. The attempts made in this current study are to extend the existing data of Bishop et al [1] to a higher impressed temperature difference with air as the working fluid and to establish further study of this configuration with water as the gap fluid.

The flow process resulting from the density change caused by a temperature gradient within the gravitational force field between concentric isothermal spheres can be represented by a mathematical model which includes a set of simultaneous, non-linear, coupled, partial differential equations subject to the associated boundary conditions. The analytic treatment of this problem is very difficult. This is due to the following reasons: (1) the non-linearity of the governing equations, (2) the invalidity of the general boundary layer approximations in this case, and (3) the lack of information of boundary conditions, especially when the flow field is not steady and

therefore not necessarily symmetrical about a vertical axis through the center of the spheres. These equations are shown in Appendix I.

The purposes of the present experimental investigation concerning the flow phenomena between concentric isothermal spheres are:

- (1) To obtain criteria for predicting the fluid-flow behavior within the gap as the radial distance and the temperature difference between spheres are varied. Both air and water are used as the enclosed fluids. These criteria will allow prediction of the type of flow which will occur under a variety of conditions.
- (2) To study the mechanism which determines when and how the onset of instability in the flow field occurs.

Furthermore, the results of this present work should contribute to a greater understanding of the natural convection process between isothermal spheres by correlating these with the existing data concerning heat transfer rates and temperature profiles. Also, the information described in this dissertation may be used as a guide to validate future analytical and numerical studies of natural convective flows in this spherical geometry.

## CHAPTER II

### LITERATURE REVIEW

Natural convection from a surface to its infinite surroundings has been studied by a number of investigators, and a rather large number of papers are available in the literature on this subject. The more recent contributions have been made relative to natural convection within enclosed spaces. However, there is still only a limited amount of information available concerning natural convective flow phenomena within confined spaces.

Good reviews of the early work concerned with the natural convection process can be found in several textbooks such as Jakob [7], Eckert and Drake [8], and Gröber, Erk, and Grigull [9]. Two things are generally agreed upon in the literature on natural convection. One is that the natural convection process is dominated by both fluid-flow and heat transfer considerations. Second is that the natural convection process within confined spaces, defined by two characteristic dimensions, can be characterized by the following dimensionless parameters:

$$N_{GR_a} = \frac{\rho^2 g \beta \Delta T a^3}{\mu^2} \quad (2-1)$$

$$N_{PR} = \frac{C_p \mu}{k} \quad (2-2)$$

and  $N_D = \frac{a}{b} \quad (2-3)$

(Actually there are two more parameters,  $\frac{g\beta a}{C_p}$  and  $\beta\Delta T$ , but these usually are not needed.) In these equations "a" and "b" are characteristic dimensions,  $\Delta T$  is a suitably defined temperature difference,  $N_{GR_a}$  is the Grashof number based on dimension "a",  $N_{PR}$  is the Prandtl number, and  $N_D$  is a dimensionless ratio of the characteristic dimensions. All the fluid properties are normally evaluated at either an arithmetic mean temperature or a volume-weighted mean temperature. An additional dimensionless group, the Rayleigh number ( $N_{RA_a}$ ), has been found convenient in certain cases to replace the Grashof number. The Rayleigh number is the product of the Prandtl and Grashof numbers:

$$N_{RA_a} = N_{PR} \cdot N_{GR_a} = \frac{\rho g \beta \Delta T a^3}{\alpha \mu} \quad (2-4)$$

In the present review, specific attention is directed toward natural convective flows between a body and its finite enclosure. For the case with small gap thickness and large radius of curvature, the spherical geometry can be approximated by a plane wall enclosure. Therefore a short review of the literature in this area is also presented for completeness. For clarity, the discussion is presented in three separated parts based on different geometrical configurations. These are (1) parallel plates and rectangular enclosures, (2) concentric cylindrical annuli, and (3) spherical annuli.

## PARALLEL PLATES AND RECTANGULAR ENCLOSURES

Usually no convective motion occurs in a fluid which is enclosed between two parallel horizontal plates with the upper plate maintained at a higher temperature than the lower. In a normal fluid for which the density decreases with temperature, such a temperature field will yield a stable situation in which the less dense layers are located above the denser fluid. Heat is transferred from the upper plate to the lower plate by conduction, and a linear temperature distribution is expected. However, when the lower plate is at the higher temperature, resulting in the less dense layer at the bottom, an unstable situation will be produced. Nevertheless, there is no convective flow before the critical Rayleigh number of 1,705 (based on the gap thickness) is reached. Upon exceeding this value the flow field will be a cellular structure with more or less regular hexagonal cells, in which the flow moves upward in the center and returns downward near the sides or vice versa depending upon the properties of the fluid. This flow situation is maintained up to a Rayleigh number of around 45,000. Above this value of Rayleigh number the flow changes to irregular turbulent. Chandra [10] found that the value of the critical Rayleigh number changes depending upon the layer thickness. It was reported by Schmidt and Saunders [11] that the length of the horizontal side of a cell was twice the layer depth. The more recent

work is that of Leontiev and Kirdyashkin [12]. They did an experimental study of flow patterns and temperature fields with 96% ethyl alcohol as the test liquid. To visualize the flow, well-wettable aluminum particles 5-20 microns in size were placed in the alcohol. They reported that polygonal structure of the flow in a horizontal layer was observed for Rayleigh numbers  $N_{RA_L} < 95,000$ . The flow in a polygonal cell is laminar with a motion of radial flow from the bounding sides of the polygon to the center. At  $N_{RA_L} \sim 10^5$ , the polygonal structure of the liquid flow ceases completely and transforms into a roller structure.

Natural convection across a closed cavity between vertical boundaries at different temperatures was studied by Batchelor [13]. He investigated this problem in three cases; (1) small Rayleigh numbers ( $N_{RA_L} < 10^3$ ) with  $H/L$  (ratio of cavity height to width) approximately unity, (2) general Rayleigh numbers with large  $H/L$ 's, (3) large Rayleigh numbers with general  $H/L$ 's. An analytical solution for the first case was found by utilizing a method of expanding the stream function and temperature in power series in terms of the Rayleigh number. He also obtained the solution for the last two cases by making drastic idealizations. He predicted transition to turbulent flow at  $N_{RA_L} = 13,700$  for air in the second case, and at  $N_{GR_L} = 10^9 (H/L)^{-3}$  for air (perhaps for other fluids also) in the last

case.

Using the same configuration, both experimental and numerical investigations were performed by Elder [14, 15]. The flow was made visible in his experimental study by using aluminum powder suspended in the fluid. The velocity measurements were made either by direct observation or from time photographs, in which the streak-length is proportional to the velocity. A steady secondary flow was observed in the interior region of the flow for  $N_{RA_L} \sim 10^5$ . Further, it was found that the secondary flows, when of sufficient amplitude, were able to generate other steady flows, called tertiary flows. Both photographs and sketches of the flow patterns were presented for various gap widths and Rayleigh numbers. In addition, the velocity profiles were also plotted for the half height along the gap at various Rayleigh numbers. His numerical solution was checked with the thermal and flow field data of Eckert and Carlson [16], and this comparison did show that both results are comparable.

Wilkes and Churchill [17] applied numerical techniques to a long rectangular channel with air as the enclosed fluid. The streamlines were obtained for Grashof numbers up to  $10^5$  and for various height-to-width ratios.

## CONCENTRIC CYLINDRICAL ANNULI

Another geometry which appears to yield flow results applicable to the study of concentric spheres is concentric cylindrical annuli. Several investigations using this configuration in natural convection have been carried out experimentally, analytically, and numerically. These studies cover a wide range of diameter ratios, Grashof numbers, and various gap fluids.

Liu, Mueller, and Landis [18] carried out an experimental study utilizing air, water, and Dow silicone fluid No. 200 as the working media. Five sets of concentric tubes, having diameter ratios ( $D_o/D_i$ ) ranging from 1.154 to 7.500, were used in their study. Different observation techniques were used for various working fluids in the gap. For air, tobacco smoke was introduced into the gap; in water, a blue-dye-water mixture was slowly injected under isothermal conditions. A small quantity of neutrally buoyant polyethylene particles added to the silicone fluid permitted visual and photographic observations. General descriptions and sketches of the flow patterns which were observed were presented.

A numerical solution to the problem of natural convective flow, with air as the medium, in cylindrical annuli was also reported in the form of plots of the stream function for the range of  $2 \leq D_o/D_i \leq 57$  and  $1 \leq N_{GR_{D_i}} \leq 10^5$  by Crawford and Lemlich [19]. Their results

are in accordance with the appropriate qualitative flow patterns obtained experimentally by Liu et al [18] at a diameter ratio  $D_o/D_i = 2.0$ .

Grigull and Hauf [20] presented numerous photographs, taken by introducing smoke to make the flow visible in a normal incident light plane, and sketches of flows. The annulus was filled with air at atmospheric pressure. Various gap width-to-inner diameter ratios ( $0.15 \leq L/D_i \leq 2.65$ ) were selected in their study. Three different types of convective flow phenomena as the Grashof number was changed were postulated. These are (1) a two dimensional pseudo-conductive regime for  $N_{GR_L} < 24,000$ , (2) a regime of transition with a three dimensional convective motion for  $24,000 \leq N_{GR_L} \leq 30,000$ , and (3) a regime of fully developed two dimensional laminar convective motion for  $30,000 \leq N_{GR_L} \leq 716,000$ .

An experimental investigation of the flow behavior for natural convection in simple and obstructed horizontal cylindrical annuli was performed by Lis [21] using the Schlieren technique. A few photographs and verbal descriptions of the flow patterns were presented in his report for various diameter ratios and Grashof numbers.

Bishop and Carley [22] carried out a photographic experimental study of natural convective flows of air between concentric horizontal cylinders. Photographs and qualitative descriptions of

the flow patterns were obtained for various operating conditions at diameter ratios ranging from 1.23 to 3.69, with temperature differences of 5°F to 100°F between the cylinders. They found two types of stable flow and one unstable flow within their range of diameter ratios. Under all temperature differences studied for diameter ratios of 1.23, 1.85, and 2.46, the first stable flow, termed a "crescent eddy" type, existed at low Grashof numbers. Another stable flow pattern, the "kidney-shaped eddy" type, was found to appear for a diameter ratio 3.69 at Grashof numbers above that at which the crescent eddy flow pattern disappeared. For higher Grashof numbers, this pattern became an unstable oscillation of the fluid in the upper region of the gap. They also found that both frequency and amplitude of oscillation were increased at increasing temperature difference.

Employing the technique set forth by Batchelor [13] to expand the stream function and temperature in an infinite series of Rayleigh number, an analytic solution, limited to low values of Rayleigh number, was reported by Mack and Bishop [23]. They found that increasing the Prandtl number above 0.70 had very little effect upon the qualitative appearance of the stream lines at low Rayleigh number, except for very small Prandtl number fluids such as liquid metals.

An extensive study of the three dimensional oscillatory flow in cylindrical annuli, observed by Bishop and Carley [22], was carried

out by Bishop, Carley, and Powe [24]. Correlation equations were given to allow estimation of the inception of this oscillatory flow and its subsequent amplitude, period, and wave length. Detailed descriptions of this particular flow phenomenon supported by photography and motion pictures also can be found in Powe [27].

Bishop and Carley [22] compared their results with these of Liu et al [18] and pointed out the very interesting possibility of obtaining different types of flows for a given diameter ratio while using different cylinder sizes. Powe [27] investigated this possibility experimentally for air within the gap as reported by Powe, Carley, and Bishop [25]. Using six different cylinder sets, two of them yielding the same diameter ratio with different cylinder sizes, and varying both the annulus pressure and temperature difference between the cylinder surfaces, they observed one steady and three unsteady flow patterns in the range of Grashof number (based on annulus width) from 300 to  $3.4 \times 10^6$ . They pointed out that radius of curvature, though not affecting the general type of the flow pattern, did affect the specific value of Grashof number at which transition from a steady to an unsteady pattern occurred. A plot categorizing the flow patterns in horizontal concentric cylindrical annuli filled with air was presented showing the transition Grashof number versus ratio of inner-cylinder diameter-to-annulus width by combining their data and several existing previous

experimental results.

The results of a numerical investigation, utilizing finite-difference techniques, to this problem were presented by Powe, Carley, and Carruth [26]. The results were compared with the existing data and excellent agreement was found. This numerical solution can also be used to predict the Rayleigh numbers where the flow will go from a stable condition to an unstable condition for a wide range of inverse relative gap widths ( $D_i/L$ ) from 2.8 to 12.5. This is due to the occurrence of steady secondary flows immediately preceding the unsteady flow, which has been observed in experimental investigations within the above specified inverse relative gap widths. It was found that a pronounced increase in magnitude of temperature and velocity components heralded the appearance of secondary flow in the large inverse relative gap widths.

#### SPHERICAL ANNULI

An initial investigation of the natural convection process in the annulus between concentric spheres was carried out by Bishop, Scanlan, and their colleagues in 1964. Since that time a series of papers have been published.

The first investigation was carried out by Bishop, Kolflat, Mack, and Scanlan [1] for air as the working medium within the gap. Using

the flow visualization techniques described in [2], they observed three different flow behaviors for diameter ratios of 1.19, 1.72, and 3.14 at various temperature differences ( $5^{\circ}\text{F} \leq \Delta T \leq 60^{\circ}\text{F}$ ). The most common pattern, the crescent-eddy type, occurred for the intermediate diameter ratio (1.72) at all temperature differences, while for the largest (3.14) and the smallest (1.19) diameter ratios it occurred only at small temperature differences. The second flow pattern, the kidney-shaped eddy type, occurred for the largest diameter ratio (3.14), i.e., the largest gap, at moderate to large temperature differences. The main difference between the first two patterns was the shape of the central-eddy region. The third flow pattern, the "falling-vortices" type, occurred at moderate to high temperature differences for the smallest diameter ratio (1.19). This flow type was unsteady and was characterized by the formation and shedding of vortex cells. Detailed descriptions and photographs concerning these three different flow patterns were also presented. Further details of this study were given by Bishop [28]. The results of an investigation of heat transfer rates and a detailed discussion of temperature distributions correlated to the observed flow patterns were presented by Bishop et al [3].

An analytical solution to this problem was carried out by Mack and Hardee [4] in the same manner as that of Mack and Bishop [23] for concentric cylinders. This solution is limited to low values of

Rayleigh number. Their highest value of Rayleigh number was considerably below the lowest value obtained experimentally by Bishop et al [3].

The two most recent reports were contributed by Scanlan, Bishop, and Powe [5] and Weber, Powe, Bishop, and Scanlan [6]. Scanlan et al [5] extended the existing heat transfer data and temperature profiles of Bishop et al [3] ( $N_{PR} \sim 0.70$ ) to include Prandtl numbers up to 4184 by introducing water and two different silicone fluids into the gap. The first investigation concerning natural convection between eccentric spheres was performed by Weber et al [6]. They introduced a conformal mapping technique to present the results of heat transfer rates between eccentric spheres to enable a comparison with the existing data for concentric spheres. A single correlation equation of heat transfer rates was obtained for an extremely wide range of diameter ratios, eccentricities, Rayleigh numbers, and Prandtl numbers. They also pointed out that the effect of a negative eccentricity (inner sphere below the center of the outer sphere) on the temperature distribution was basically an enhancement of the convective motion, while a positive eccentricity tended to stabilize the flow field and promote conduction rather than convection. The multicellular flow pattern, which has previously been postulated by Bishop et al [3] to explain the temperature distribution between concentric spheres with small gap spacing, was

also found to yield a plausible explanation for the thermal field obtained using the largest inner sphere ( $D_i = 9''$ ) considered in their investigation.

In addition, natural convection heat transfer between isothermal centrally located vertical cylinders and their isothermal spherical enclosure was experimentally investigated by Weber [29]. Various diameters of cylinders and aspect ratios, defined as the ratio of length of straight cylindrical section to radius of cylinder, were used in his study with the gap filled with water. Based upon his measured heat transfer rates and temperature distributions, he noted that the larger aspect ratios for all diameter ratios seemed to curtail the convective activity while the smaller aspect ratios for all diameter ratios seemed to promote convective activity. A multicellular flow regime was also postulated for the smallest diameter ratio cylinder investigated.

## CHAPTER III

### EXPERIMENTAL APPARATUS AND PROCEDURE

#### EXPERIMENTAL APPARATUS

The apparatus used in this investigation was designed to provide the capability to study the characteristics of natural convective flow between isothermal concentric spheres with different diameter ratios using both air and water as the gap media. A photograph of the assembled apparatus, utilizing water as the gap fluid, is shown in Figure 1. Figure 2 and Figure 3 present schematics of the entire operating system for water and air as the gap working fluid respectively. An equipment list is provided in Appendix II for reference purposes.

The same inner spheres, 9.00, 7.00, 5.50 and 4.50 inches in diameter, used in the heat transfer study by Scanlan et al [5] were also used in the current study. All of the inner spheres were fabricated from copper with an approximate wall thickness of 0.025 inch. In order to establish the flow visualization, a glass outer sphere was fabricated from two hemispheres with an inner diameter of 9.77 inches. The combination yielded diameter ratios ( $D_o/D_i$ ) of 1.09, 1.40, 1.78, and 2.17 which are close to the values used in the heat transfer study of Scanlan et al [5]. This arrangement will allow convenient correlation between thermal and flow phenomena for this geometry.

The inner spheres were supported in the outer sphere by a

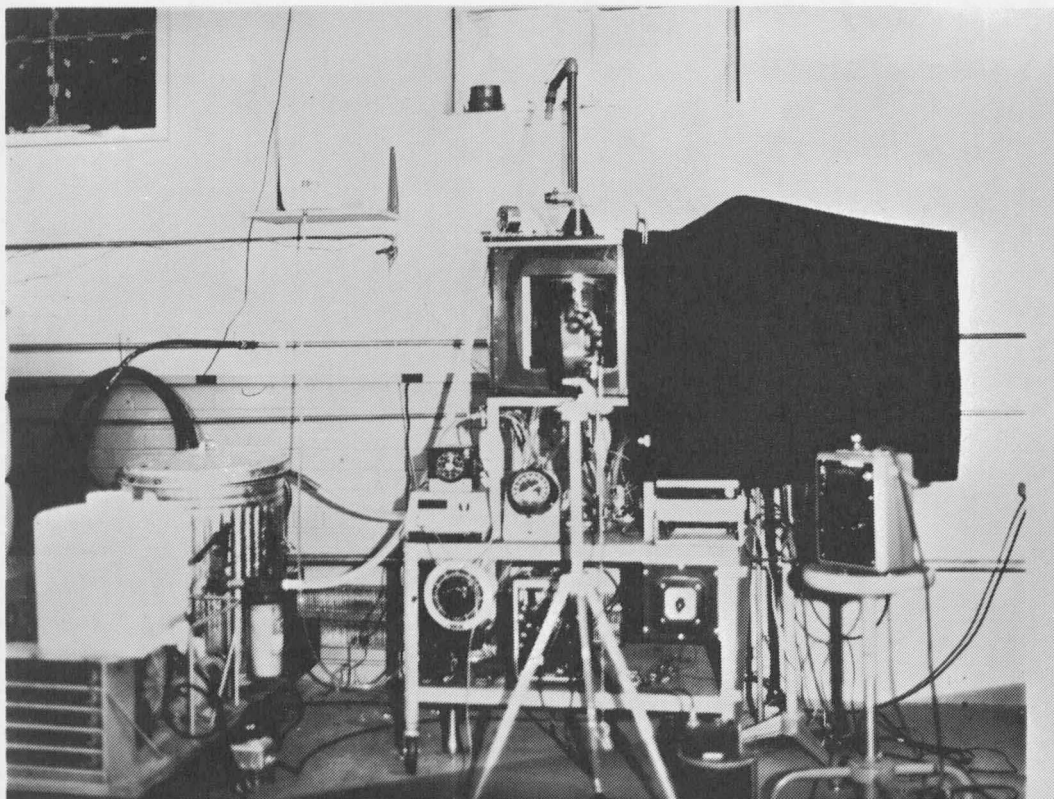


Figure 1. Assembled Apparatus with Water Cooling System

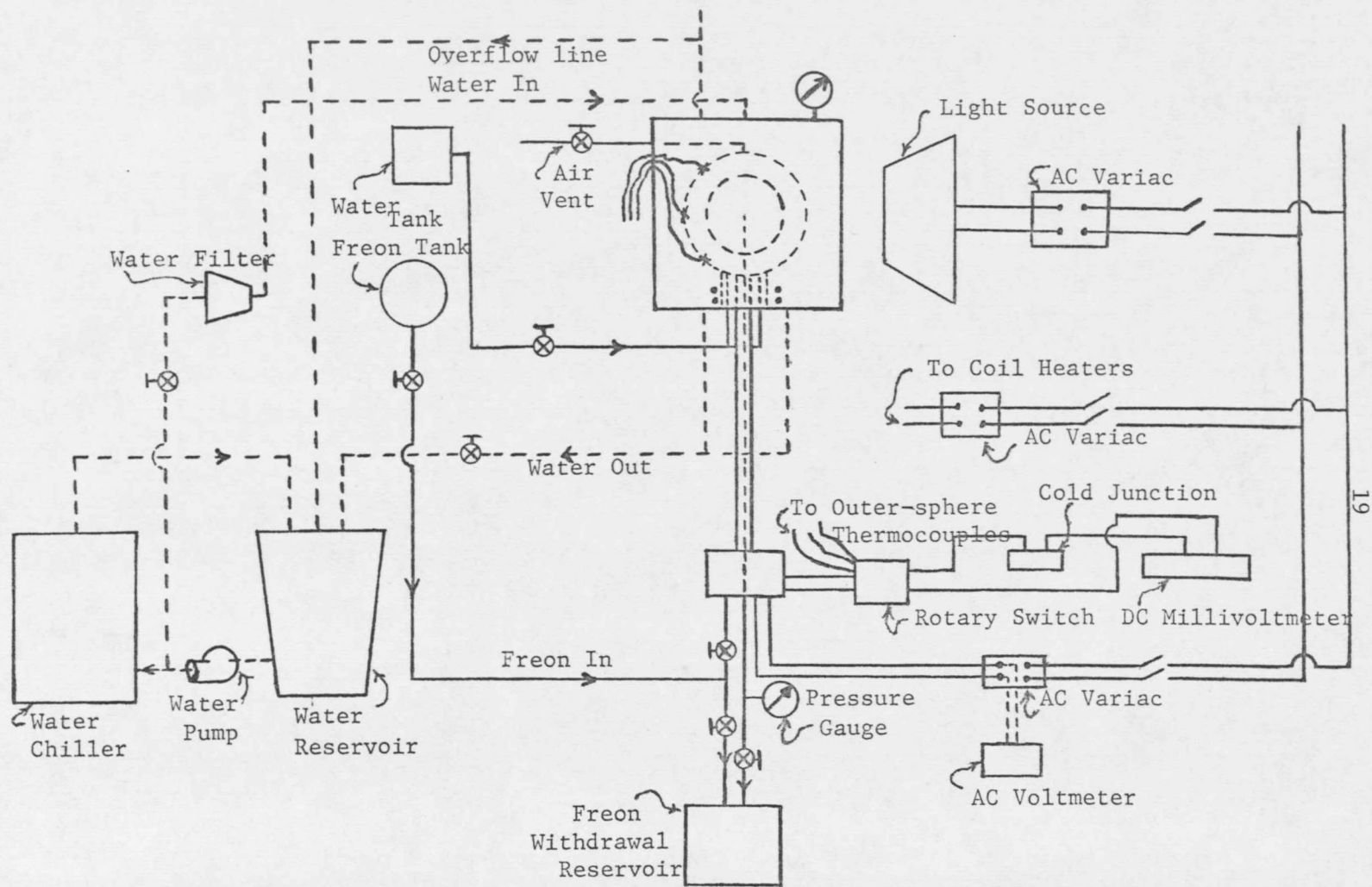


Figure 2. Schematic Diagram of Experimental System (Water as Gap Fluid)

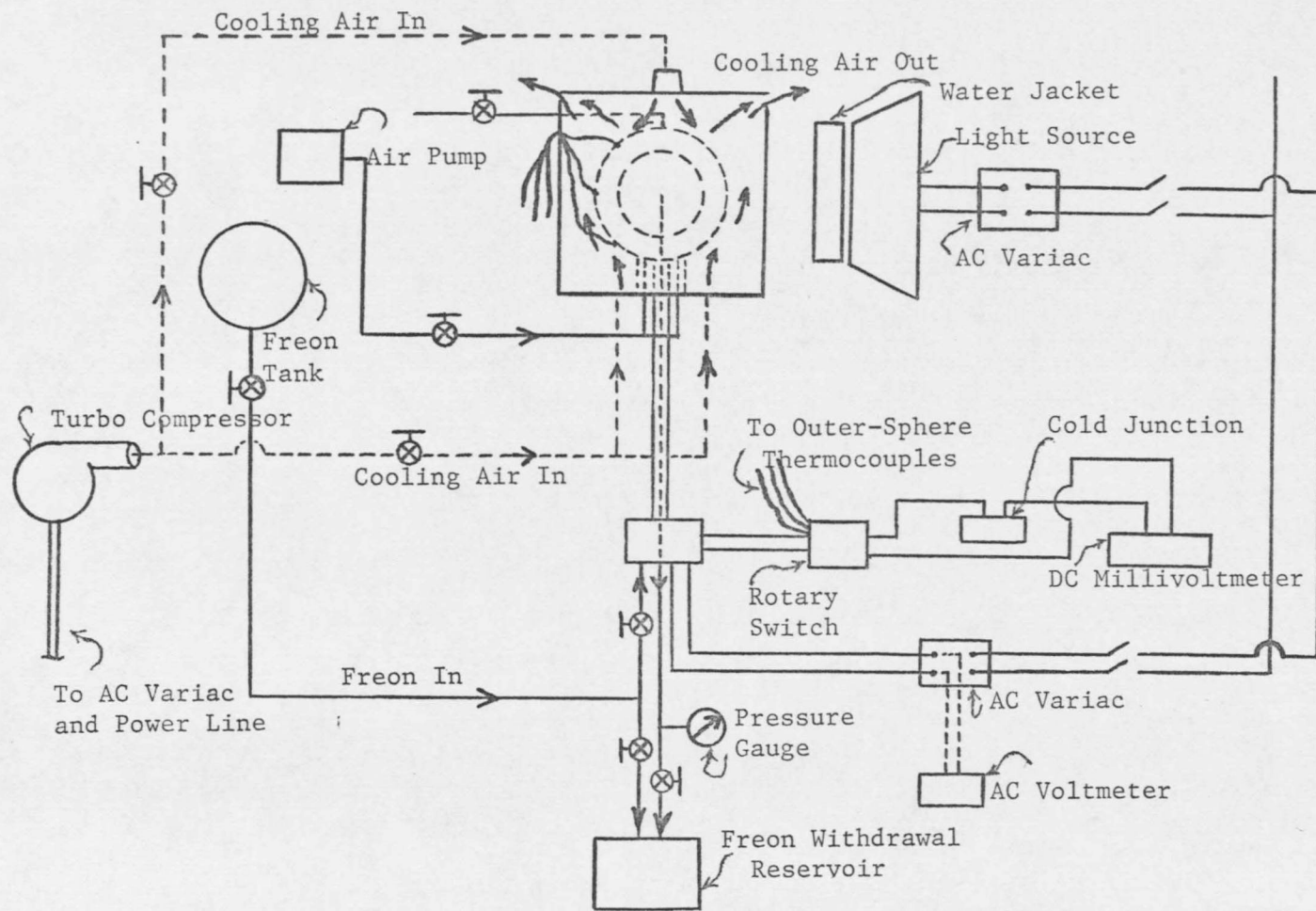


Figure 3. Schematic Diagram of Experimental System (Air as Gap Fluid)

stainless steel stem of 0.05 inch diameter and 0.065 inch wall thickness. The stem was insulated by using a plastic shrink tube to minimize lateral heat conduction through the tube. The stem, in addition to providing support for the sphere, served as a support for the electrical disk heaters and as a transfer tube for the power leads, thermocouples, and liquid Freon-11. Initially, the inner sphere was approximately half filled with Freon liquid and half with Freon vapor. The level of the Freon liquid could be controlled by a small stainless steel tube which acted as both a stand pipe for venting during the Freon-11 charging and as a means of measuring pressure within the inner sphere. The isothermal inner-sphere temperature was achieved by passing an electric current through the heater, which was located below the liquid level, causing a continuous Freon vaporization-condensation cycle. By varying the setting on an AC Variac located in the heater circuit, various inner sphere temperatures could be obtained. Figure 4 shows the arrangement of power leads, heaters, thermocouples, etc. inside the inner sphere.

The outer sphere consisted of two glass hemispheres with the separating plane located at an angle of 30 degrees with respect to the vertical axis. The hemispheres were joined together using a silicone sealant which yielded leak-proof sealing and ease of disassembly for changing the inner sphere. The inner diameter and

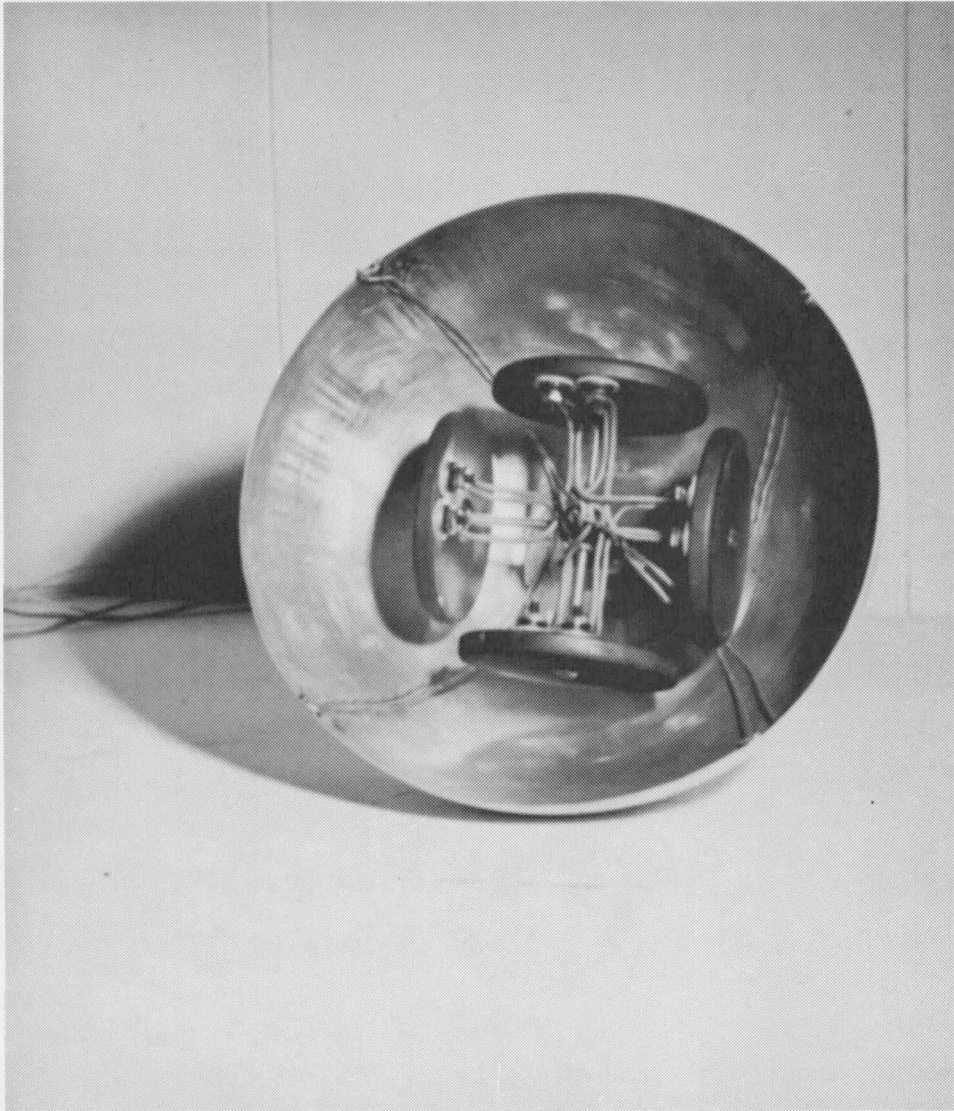


Figure 4. Interior of inner sphere

thickness of the glass sphere were 9.77 inches and 0.21 inch respectively. A 0.20 inch hole at the top served as an air vent while filling the gap with water. Another hole, 1.50 inches in diameter and located at the bottom, provided space for the stem of the inner body and a means of injecting the gap fluids. A 3.5 inch by 3.5 inch cylinder made of plexiglass was attached to the bottom of the glass sphere using epoxy cement. A tapered hole through the cylinder provided angular deflection of the stem permitting installation of the larger diameter inner-bodies. Figure 5 shows the two glass hemispheres. The installation of the inner sphere is illustrated schematically in Figure 6. The separating plane of the two hemispheres was rotated through an angle of  $45^\circ$  with respect to a front view before attaching the sphere to its plexiglass cubical enclosure. This prevented the plane from obstructing the flow visualization.

The cubical enclosure was made of plexiglass and has a characteristic length of 18 inches with a wall thickness of 0.5 inch. The enclosure was designed with a removable top cover for changing the spheres. The supporting cylinder of the glass sphere was mounted to the bottom of the enclosure using screws. In order to minimize optical reflections, the inner surfaces of the cubical enclosure were lined with thin phenolic sheets painted flat black with the exception of the viewing angle and a 0.2 inch lighting slit. The

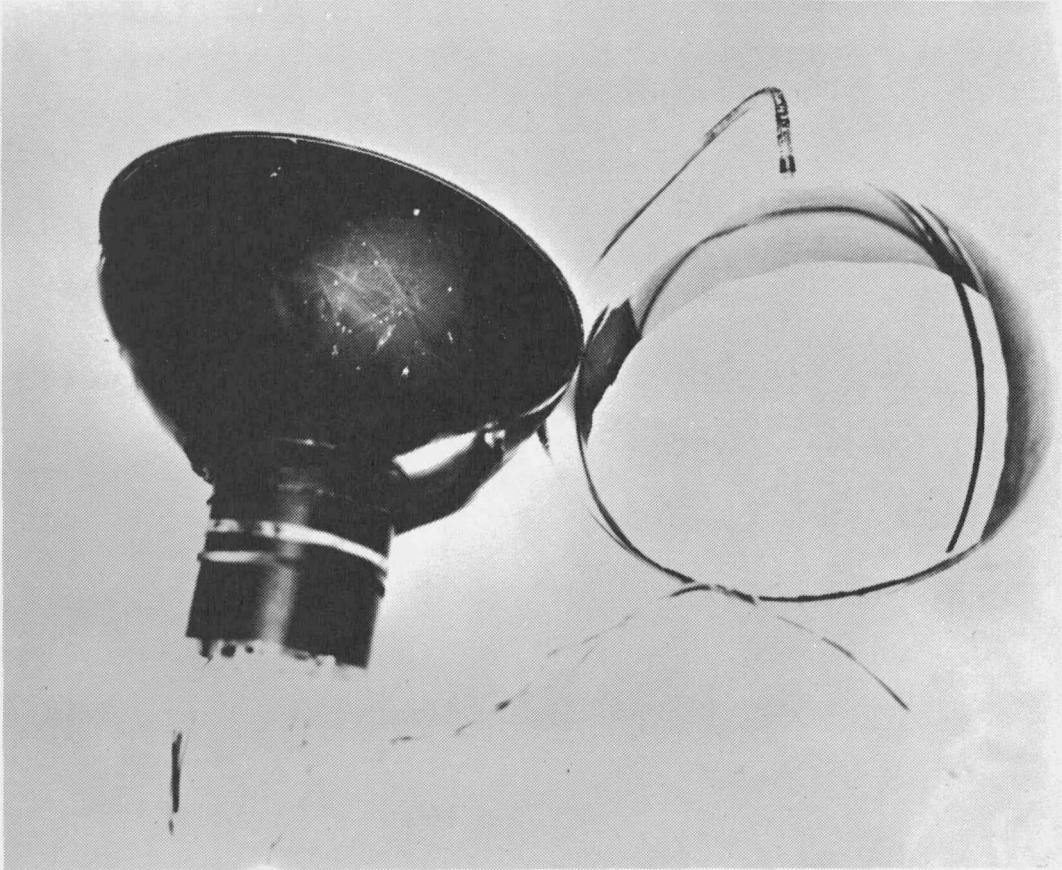


Figure 5. Glass Hemispheres

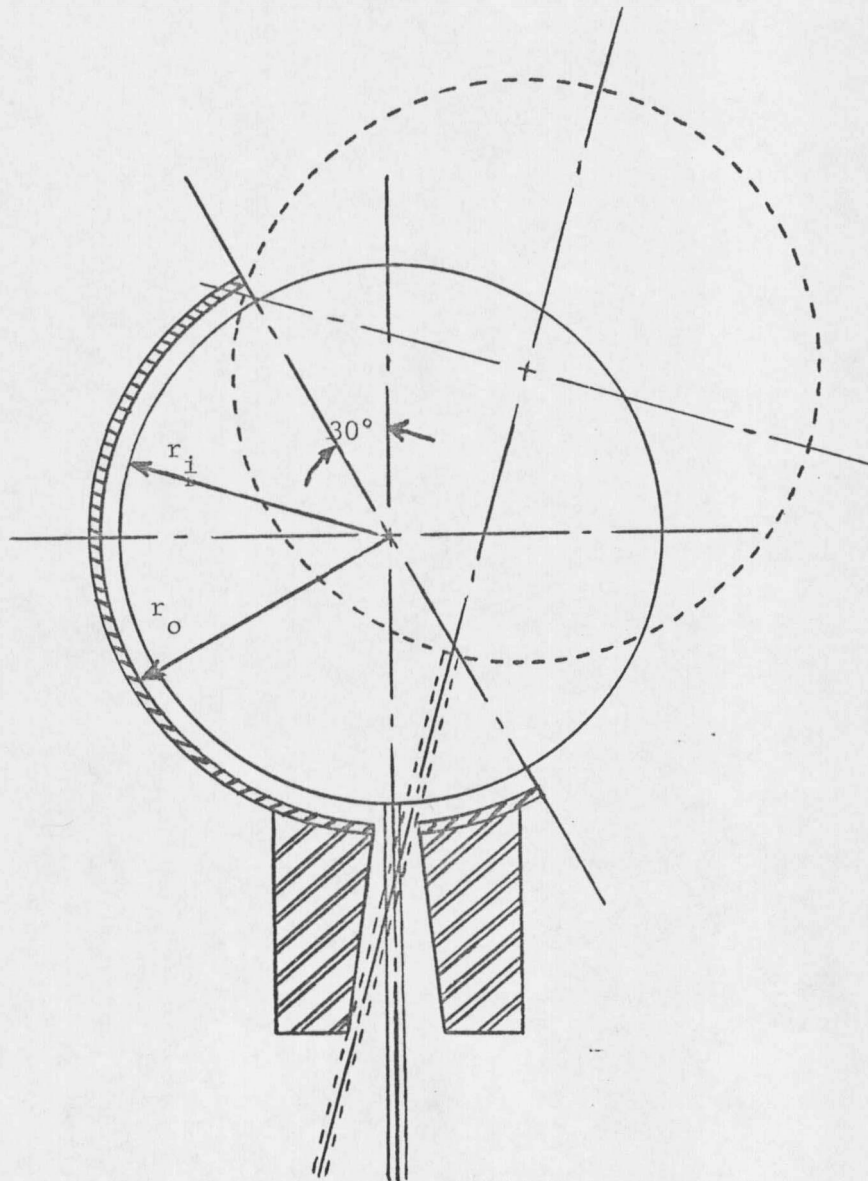


Figure 6. Installation of Inner-Sphere  
in the Glass Sphere

outer surface of the inner sphere and the majority of the inner and outer surfaces of the glass sphere were also sprayed with a thin black layer for the same purpose.

Both inner and outer sphere temperatures were monitored using copper-constantan thermocouples placed at various locations on the sphere surfaces. The thermocouples for the inner sphere were placed in the seam of the two hemispheres prior to final assembly. Six thermocouples, imbedded the depth of the wall thickness, were attached to the glass sphere with epoxy cement. The arrangement of the thermocouple locations was chosen such that during testing, it could be determined whether the sphere was being isothermally maintained. The surface temperature of the outer sphere was taken to be the average of these six thermocouple readings.

The cooling system used to maintain the isothermal condition of the glass sphere was determined by the gap fluid used. For air as the gap working fluid, a forced air draft was introduced into the cubical enclosure and was passed over the glass sphere from both the top and the bottom of the enclosure. It was withdrawn through a narrow gap underneath the edges of the top cover. The air draft was supplied by a turbo-compressor whose speed was regulated by an AC Variac. The flow rates of the top and the bottom manifolds were adjusted by metering valves on each air line. This arrangement

eliminated the problem of flow separation of the cooling air while passing over the glass sphere. The isothermal condition was then achieved by proper adjustment of the compressor speed and flow rates from each air line.

For water as the gap working fluid, a closed cooling system which included a reservoir, pump, water filter, chiller, and an overflow discharge line was used and operated with a flow rate of 5 GPM. The cooling water was introduced into the enclosure from the top and withdrawn from the bottom through a manifold system. A thin plexiglass cylinder, 12 inches in diameter, was placed inside the cubical enclosure surrounding the glass sphere. This resulted in achieving an increased velocity of the cooling fluid passing over the sphere.

It was necessary to fill the remaining space in the enclosure with water for flow observation to remove geometric optical distortion. This provided a plane surface through which the flow could be observed without the distortion caused by refraction at the curved water-glass-air interfaces. The supporting cylinder of the glass sphere was surrounded by two coil heaters connected to an AC Variac. During the operation of the cooling system, a certain amount of energy was supplied to these coil heaters. By doing this a cooling problem caused by a large variation of local heat transfer

rates along the inner surface of the glass sphere, caused by poor thermal conductance of the glass sphere, was minimized

The inner-sphere support stem passed through the outer sphere, a tapered hole and plug sealing device, and the cubical enclosure to connect to a small reservoir made of stainless steel. For sealing purposes, two O-rings were placed between the inner-sphere support tube and tapered plug, and two were placed between the tapered plug and the tapered hole in the outer-sphere support cylinder. The small stainless steel reservoir permitted the emergence of power leads, thermocouples, and standpipe by means of Conax fittings to provide leak-free integrity of the system. The reservoir also housed the Freon-11 fill port and the junction of the Freon-11 pressure gage. The reservoir rested on a threaded rod that allowed vertical adjustment of the inner sphere. The inner sphere could be accurately positioned within the outer sphere by utilizing a scale located beside the reservoir.

A light-tight box containing two 650 watt, air cooled, high intensity, quartz-iodine lamps provided a thin collimated plane of light for illumination of the annulus to enable flow visualization and photography. In conjunction with the use of tracers, this allowed the observation of the flow patterns occurring in a plane by viewing the spheres at right angles to the collimated light beam.

The tracers were introduced into the illuminated plane through four small tubes positioned beside the inner-sphere support-stem. For air as the gap medium, a preliminary observation indicated there was an effect on the flow patterns due to the radiant energy from the light beam. The same observation was also noted by Bishop and Carley [22] and Powe [27]. This effect was eliminated by passing the light through a 0.75-inch thick water plane when air was the working fluid. The circulating cooling water in the cubical enclosure served this same purpose during the studies using water as the gap fluid.

The introduction of tobacco (cigar) smoke into the spherical annulus was the flow visualization technique employed for air as the working fluid. For water as the working fluid, however, satisfactory tracers were unavailable. The ideal tracers for use in water should have the following characteristics:

- (1) The tracer element must be neutrally buoyant with time and temperature variation,
- (2) The tracer element must be visible and photographable,
- (3) The tracer element must follow and indicate the actual physical flow phenomena.

In order to study the flow phenomena with water in the annulus, a special visualization technique was developed in the current study. The working fluid with the tracer was prepared in the following

manner:

- (1) The needed quantity of distilled water was boiled.

The purpose of this was to deaerate the water in order to minimize bubble collection on the inner surface of the glass sphere. Previously, these air bubbles caused the view of the flow to be partially obstructed.

- (2) The boiled water was cooled to approximately 80°F.

- (3) This water was then siphoned into a storage container to which was added a very minute amount of liquid detergent (3 gallons of water to approximately 15 drops of "Ajax"). Gentle shaking of the container was necessary to form a homogeneous mixture without introducing any air bubbles.

- (4) After sitting several hours, numerous very small neutrally buoyant particles were observed in a lighted plane. Having obtained this condition, the mixture was introduced into the gap. Figure 7 shows these particles at rest within the spherical annulus before heating.

It was found that the concentration of particles was affected by the quantity of detergent added. Too much detergent caused the water to appear milky grey which reduced the contrast significantly.

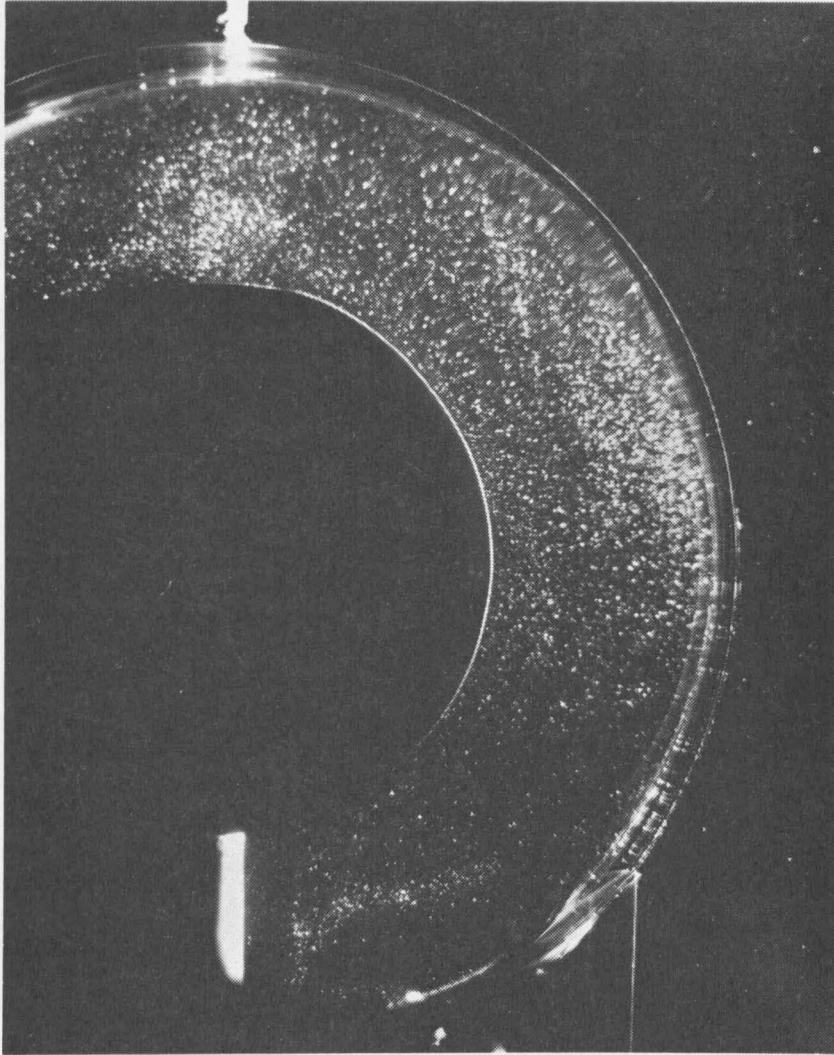


Figure 7. Particles in Water Within the Spherical  
Annulus Before Heating

It was also discovered that when the temperature of the mixture exceeded 120°F, the number of particles observed was considerably reduced. This visualization technique could very well prove useful for flow studies in other fields where water is the working medium.

Several different kinds of solid particles used by previous investigators were evaluated in the current study. Some of these were aluminum powders, polyethylene, polystyrene, and a type of small, hollow glass spheres called Eccospheres. All of these particles revealed the following disadvantages.

- (1) They were not neutrally buoyant for a long period of time under the necessary variation of water temperature.
- (2) Since the spherical annulus was an enclosed space, many particles were found to adhere to the inner surface of the glass sphere causing visual obstruction.
- (3) In comparison to the detergent particles, most of the particles had poorer optical reflectivity and therefore were much more difficult to photograph.

Another flow visualization technique described by Baker [30] was also evaluated. A solution, prepared by adding a small amount of thymol blue PH indicator to distilled water, was introduced into the annulus. A blue dye was created in the gap upon impressing a small DC voltage between two electrodes within the solution. This method

proved unsuccessful because the contrast between the blue dye and the red solution was rather difficult to distinguish.

Still photographs of the flow patterns were obtained using a tripod-mounted 4"x5" Calumet Camera, and motion pictures were taken by use of a Beaulieu R 16mm "Automatic" photographic recorder. Fast film was selected due to the adverse lighting conditions. Kodak 4-X Reversal, 7277 16mm movie film was used for the motion pictures. All of the still photographs were taken with either Kodak Tri-X Pan Professional Film or Polaroid Black & White 3,000 speed Land film. In order to achieve good contrast, kodabromide F·4 print paper was used for enlargement and printing.

## EXPERIMENTAL PROCEDURE

The desired inner sphere was selected and painted black before placing it within the glass outer sphere. A single-component, air-curing silicone sealant was used to join the two glass hemispheres. A leak-proof seal was obtained by allowing approximately 24 hours for the sealant to cure. The spheres were then installed within the cubical enclosure, followed by connection of the electrical power, thermocouples, and plumbing. The concentric location of the inner-sphere was ensured by the following simple procedure:

- (1) Raising the inner sphere to its extreme upper location and recording the reading of the scale indicated by a needle mounted on the stem;
- (2) Lowering the inner sphere to its extreme lower location and recording its corresponding reading; and
- (3) Setting the inner sphere at the middle position between these two marks.

The Freon-11 fill and vent valves were opened. Both valves were then closed when a steady Freon-11 stream emerged from the vent line, which indicated the inner sphere was half full.

The following procedures were followed for water as the gap working fluid:

- (1) The prepared working fluid was introduced into the

annulus from the container by gravity flow.

- (2) As soon as the annulus was completely filled, the inlet valve was closed. The air vent was kept open to allow for thermal expansion of the fluid.
- (3) The cooling system and AC Variac connected to the heaters in the inner sphere were turned on. The voltage was adjusted to yield the desired temperature.
- (4) Power supplied to the coil heaters was then varied such that the inner surface of the enclosing sphere approached an isothermal condition.
- (5) Allowing sufficient time for thermal equilibrium to be reached, the gap-flow phenomena were then investigated.

The following procedures were followed for air as the gap working fluid:

- (1) The annulus was opened to the atmosphere through a smoke introducing valve.
- (2) The AC Variac was adjusted to give the desired inner sphere temperature.
- (3) The cooling fan was turned on and adjusted in speed. The upper and lower air flow rates were regulated by valves in the air lines to obtain the desired outer

sphere temperature.

- (4) When thermal equilibrium was reached, cigar smoke was gently introduced into the gap. Before the flow pattern investigation, sufficient time was allowed to insure that the flow field was fully developed. It was found that the smoke density in the annulus affected only the pattern contrast and did not affect the flow pattern itself. Therefore the amount of smoke introduced into the annulus depended upon visual and photographic considerations.

Visual observation and photographs were made for each temperature difference achieved. A written description and motion pictures were also recorded for each type of flow pattern. In addition, the following data were recorded with each observation, photograph, and motion picture taken:

- (1) Gap fluid,
- (2) Gap pressure (for air only),
- (3) Inner-sphere temperature,
- (4) Outer-sphere temperature,
- (5) Inner and outer sphere diameters,
- (6) Heater voltage, and
- (7) Run number.

The gap working media and associated geometric combinations in

the present investigation are shown in Table 1.

TABLE 1

## GAP WORKING FLUID AND ASSOCIATED GEOMETRIC COMBINATIONS

Gap Working Fluid	Air			Water			
$D_o$ (in)	9.77			9.77			
$D_i$ (in)	4.50	5.50	7.00	4.50	5.50	7.00	9.00
$D_o/D_i$	2.17	1.78	1.40	2.17	1.78	1.40	1.09
$L/D_i$	0.59	0.39	0.20	0.59	0.39	0.20	0.04

## CHAPTER IV

### EXPERIMENTAL RESULTS AND DISCUSSION

From the data recorded, as stated in the previous chapter, for each of the flow patterns, the appropriate dimensionless parameters such as diameter ratio, relative gap thickness ( $L/D_i$ ), Grashof number, Prandtl number, and Rayleigh number were calculated. The gap thickness, inner diameter, and inner radius were selected as the characteristic dimensions in the calculation of certain dimensionless parameters. Since a large amount of data was involved in this investigation, a data reduction program, written for the Xerox Data Systems Sigma 7 digital computer, was utilized to calculate thermocouple temperatures and properties of the gap working fluid and then to obtain the dimensionless parameters. A complete listing of this program for water as the gap working fluid and sample results from this program are found in Appendix III. For air as the gap working fluid, a listing of the data reduction program can be found in Powe [27]. In this data reduction process, all fluid properties, being temperature dependent, had to be evaluated at some suitable reference temperature. Previous investigations [5, 28] have demonstrated satisfactory results by utilizing the volume weighted mean temperature,  $T_{vm}$ , which is defined as:

$$T_{vm} = \frac{[(r_{avg}^3 - r_i^3)T_i + (r_o^3 - r_{avg}^3)] T_o}{r_o^3 - r_i^3} \quad (4-1)$$

The physical interpretation of this mean temperature can be explained in the following manner: This temperature is determined by treating the fluid contained between the inner sphere and an imaginary sphere, of diameter equal to the arithmetic mean diameter of the inner and outer spheres, as being at the inner sphere temperature and the fluid contained between the imaginary sphere and the outer sphere as being at outer sphere temperature. An additional reference temperature was also employed. This was an arithmetic mean temperature defined as:

$$T_{am} = \frac{T_i + T_o}{2} \quad (4-2)$$

For clarity, this chapter is presented in three sections; the flow pattern descriptions, the summary of experimental results, and the discussion of results. All those dimensionless parameters employed in this chapter are based upon gap thickness (L) as the characteristic dimension, and the fluid properties, being temperature dependent, are evaluated at the volume weighted mean temperature ( $T_{vm}$ ) except when otherwise indicated. The term minimum observable value of Grashof

number used in this chapter is defined as the value corresponding to the smallest temperature difference ( $\Delta T \sim 5^\circ\text{F}$ ) for a given fluid and diameter ratio. The limiting value of the temperature difference was chosen such that any error introduced due to slight temperature variation on the spheres would be negligible.

#### FLOW PATTERN DESCRIPTIONS

This section is presented in such a manner as to give a detailed description of each flow pattern which was observed in the spherical annulus for increasing temperature differences with each diameter ratio. These descriptions are also supported by still photographs, motion pictures, and sketches. The results for both air and water as the gap working fluid are treated in two sub-sections.

#### AIR AS THE GAP WORKING FLUID:

The first spherical configuration utilized in this investigation consisted of a 4.50 inch diameter inner sphere and 9.77 inch diameter outer sphere, yielding a diameter ratio of 2.17 and a relative gap thickness ( $L/D_i$ ) of 0.59. For a Grashof number ( $N_{GR_L}$ ) above a minimum observable value of 72,000 ( $N_{RA_L} = 51,000$ ) and below approximately 166,500 ( $N_{RA_L} = 118,000$ ), a steady "crescent eddy" pattern was observed in the annulus. In the crescent eddy pattern, shown in Figure 8, the fluid immediately adjacent to the

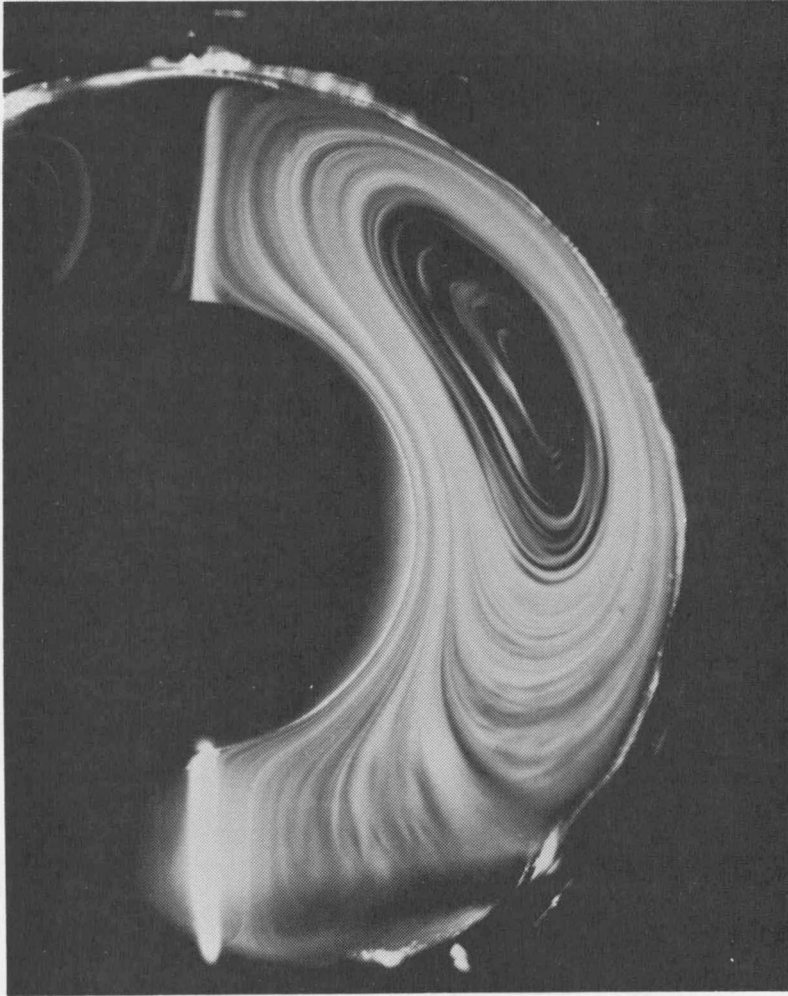


Figure 8. Steady Crescent Eddy Pattern for

$$D_o/D_i = 2.17$$

$$L/D_i = 0.59$$

$$N_{GR_L} = 72,000$$

$$N_{GR_L} = 51,000$$

spheres flows with a relatively large speed compared to that in the central and major part of the gap. Flow was upward along the inner sphere and downward along the outer sphere. The upward flow region was slightly thicker than the downward flow region. A distinct center of the crescent eddy was seen to be located above the horizontal and near the outer sphere. In the upper region of the gap, there was a distinct vertical dividing line, or chimney, between the two halves of the pattern. The flow did not extend completely into the lower region of the annulus, and this resulted in a relatively stagnant region. The downward flow along the outer sphere partially entered and expanded into this stagnant region. Meanwhile the fluid was also withdrawn from this region and converged into a thin layer as it moved upward along the inner sphere. This stagnant region appeared to decrease slightly in size as the Grashof number was increased. It was also observed that the location of eddy center moved radially outward and upward in angular position for an increase in Grashof number.

As shown in Figure 9 for a Grashof number of 166,500 ( $N_{RA_L} = 118,000$ ), a small distortion emerges at the lower portion of the central low-speed region. The central flow region, shown in Figure 10 has become distorted into a kidney shape, as the value of Grashof number was increased. This kind of flow pattern was named

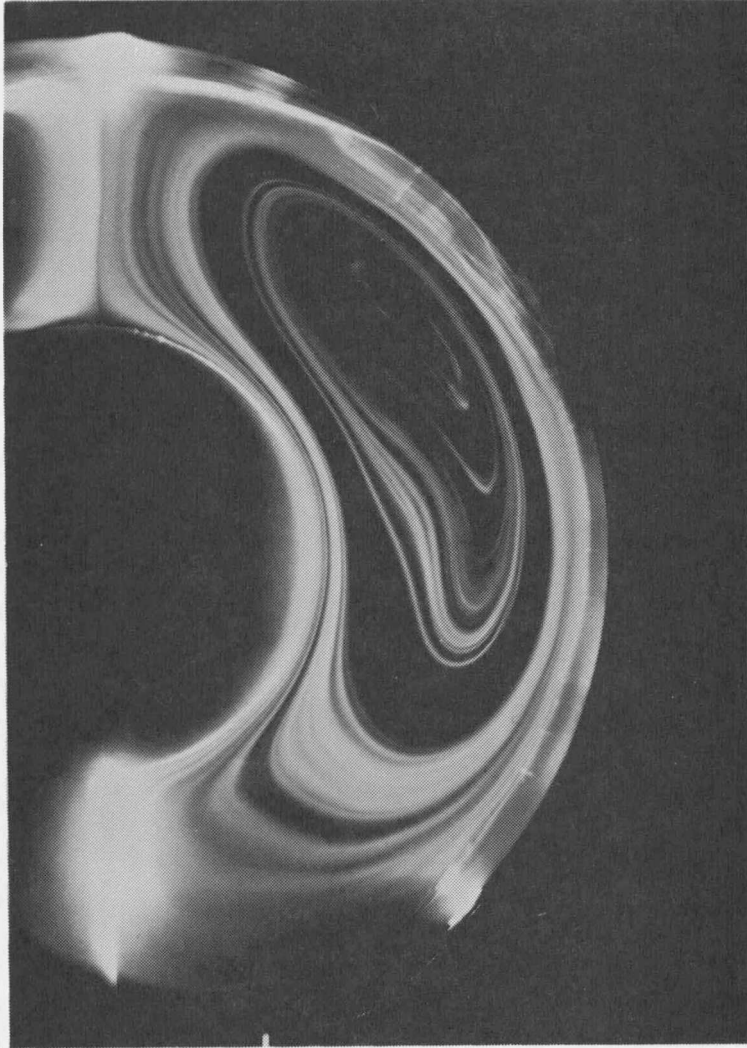


Figure 9. Photograph Showing Onset of Steady  
Kidney-Shaped Eddy Pattern for

$$D_o/D_i = 2.17$$

$$L/D_i = 0.59$$

$$N_{GR_L} = 166,500$$

$$N_{RA_L} = 118,000$$









































































































































































